Three-Dimensional Compatible Sacrificial Nanoimprint Lithography for Tuning the Wettability of Thermoplastic Materials

Three-Dimensional Compatible Sacrificial Nanoimprint Lithography for Tuning the Wettability of Thermoplastic Materials

Molla Hasan[1], Imrhankhan Shajahan[1], Manesh Gopinadhan[2], Jittisa Ketkaew[3], Aaron Anesgart[4], Chloe Cho[4], Saransh Chopra[4], Michael Higgins[4], Saira Reyes[4], Jan Schroers[3], Chinedum O. Osuji[2,5], Jonathan P. Singer[1*]

[1]Department of Mechanical and Aerospace Engineering, Rutgers University, New Jersey

[2]Department of Chemical and Environmental Engineering, Yale University, Connecticut

[3]Department of Mechanical Engineering and Materials Science, Yale University, Connecticut

[4]New Jersey Governor's School of Engineering and Technology, Rutgers University, New Jersey

[5]Department of Chemical and Environmental Engineering, University of Pennsylvania, Pennsylvania

Abstract

We report the tuning of surface wetting through sacrificial nanoimprint lithography. In this process, grown ZnO nanomaterials are transferred by imprint into a metallic glass and an elastomeric material, and then etched to impart controlled surface roughness. This process increases the hydrophilicity and hydrophobicity of both surfaces, the $Pt_{57.5}Cu_{14.7}Ni_{5.3}P_{22.5}$ metallic glass and thermoplastic elastomer, respectively. The growth conditions of the ZnO change the characteristic length scale of the roughness, which in turn alters the properties of the patterned surface. The novelty of this approach includes reusability of templates and that it is able to create superhydrophilic and superhydrophobic surfaces in a manner compatible with the fabrication of macroscopic 3D parts. Because the wettability is achieved by only modifying topography, without using any chemical surface modifiers, the prepared surfaces are relatively more durable.

*Corresponding Author
Jonathan P. Singer
jonathan.singer@rutgers.edu
Mechanical and Aerospace Engineering
98 Brett Road
Piscataway, NJ 08854

1.0 Introduction

Wettability is a functional property of solids which is important from the aspect of fundamental physics and practical applications. Controlling wettability triggers a plethora of emerging applications ranging from household self-cleaning surfaces to advanced fields, including smart filters [1], corrosion resistance materials [2], and anti-fogging surfaces [3]. Comprehensive reviews on incongruous wetting behavior (including full wetting and anti-wetting) and applications of special wettable materials can be found in Refs [4-7]. To understand the physics of wetting (both statics and dynamics) thoroughly, 2D surfaces are sufficient. However, for real-world engineering applications such as filtration [8,9], anti-icing [10,11], condensation control [12,13], and biomimetic water striding [14,15], it is crucial to induce special wettability in 3D monoliths. Few studies demonstrated superhydrophobic bulk materials [16,17], but the scope of thermoplastic materials as a 3D superhydrophobic monolith is less explored.

Although surface chemistry and surface roughness can control the surface wettability individually, dual-effect of chemistry and roughness is essential to render a surface superhydrophobic or superhydrophilic. High-surface energy materials such as metals and semiconductors facilitate extreme wetting. Conversely, polymeric materials are suitable for making superhydrophobic surfaces because of their low surface energy and facile fabrication of single and dual-scale roughness that maintains a heterogenous wetting state [18]. According to Wenzel's hypothesis, hydrophilic metals and hydrophobic polymers can be turned into superhydrophilic and superhydrophobic, respectively through topographic modification [18-23]. Numerous techniques that are developed for micro- and nanostructures fabrication, including molding lithography [24-29], etching [30,31], phase separation [32,33], diffusion-limited growth [34,35], and self-assembly [36,37], have been utilized for making superhydrophobic surfaces.

These methods are less compatible for patterning 3D objects, however, and as a result, it is difficult to render superhydrophobicity in 3D materials. Therefore, scalable surface texturing methods are of great interest to the functionalization of these surfaces.

Nanoimprinting has emerged as an effective route to change the wettability of materials because it is simple and easy to control the surface topography [38-40]. In this method, first, nanostructures generated via some other lithographic process on a master template are transferred to desired materials' surfaces through either a thermoplastic-, etching-, or photoresin-based forming. Second, the surfaces are optionally modified with low-surface energy materials. These low-surface energy materials can enhance the hydrophobicity of a surface; however, their effectiveness is reduced substantially due to low chemical resistance and physical resistance over time [41]. Moreover, these materials are usually toxic and expensive, which also limits the practical applications of superhydrophobic surfaces. For instance, low-surface energy fluorocarbon materials are contaminants because of their decomposition into perfluorooctanoic acid [42], which is potentially toxic to humans [43,44]. Therefore, rendering superhydrophobicity tuning merely the topography of materials has attracted tremendous interests recently [45,46].

We recently introduced sacrificial nanoimprint lithography (SNIL) of hydrothermally-grown ZnO nanostructures as a means to impart nanostructures to thermoplastically-formed surfaces [28]. Hydrothermal synthesis is a chemical process that permits the seeded growth of ZnO nanostructures on various substrates at low temperature (~ 90 ^{o}C) [47-49]. This method allows growing nanostructures on a large area with various morphologies by controlling the growth conditions, e.g., seed layer, growth solution composition, and temperature. The seed layer precursor for growing ZnO nanostructures is often nanoparticles; however, dense nanostructures

can also be grown on other metallic substrates without using any additional treatment [50,51]. One attractive feature of this latter property is that brass and aluminum, both common mold materials for thermoplastic forming, can be used to grow ZnO [28,52]. In SNIL, these structures are simultaneously imprinted and transferred to the molded material during thermoplastic forming and separation. As ZnO is amphoteric, it can then be easily removed in mild acid or base. In our previous work, we demonstrated the wide variety of morphologies possible on even 3D microstructures of thermoplastically-formed metallic glass (MG) created by the SNIL process [28].

In this study, we investigate the use of ZnO SNIL to modify the surface wetting of two different types of thermoplastic materials: (1) MG and (2) thermoplastic elastomer (TPE), through SNIL. MGs have emerged as a representative metal to study the topography-wetting correlation of high energy materials [53-59]. Previous studies focus on hydrophilic to hydrophobic transition, but the potential of MGs used as a superhydrophilic materials has not been investigated, and here we show that SNIL can induce superhydrophilicity in MGs. TPEs are widely used for a range of thermoplastically-formed consumer goods, and we also show that this method is also adaptive to tune the wettability of these polymeric materials. Importantly, we demonstrate that this method is scalable to make large 3D superhydrophobic parts.

2.0 Experimental Procedure

Nanoimprint lithography is a top-down and high-throughput surface patterning method in which the surface morphology of a template is replicated oppositely into a pliable material through embossing (hot or cold). In this study, we have used ZnO nanostructures as a sacrificial template, enabling the SNIL fabrication of nanostructures in different thermoplastic materials.

2.1 Making Template with ZnO Nanostructures

The Pt-based MG samples (hereafter referred as Pt-MG) employed in this study were the same structures as used in Ref. [60]. Their synthesis is described in that manuscript. For TPE studies, ZnO nanostructures were grown on aluminum templates by hydrothermal method (Fig. 1a). First, an aluminum template was cleaned ultrasonically with acetone, ethanol, and deionized water, in that order. Then, the template was etched by 0.1 M KOH solution for 0-40 minutes depending on the desired roughness of the template surface. Afterward, it was washed by a stream of deionized water and dried in air. Second, the growth medium was prepared by dissolving 0.00625 M zinc acetate dihydrate (Sigma-Aldrich, >98%) and 0.025 M hexamethylenetetramine (HMTA) (Sigma-Aldrich, >98%) in a solution of deionized water. Finally, to grow the ZnO nanostructures, the template was attached to a glass slide right-side-down using adhesive and submerged in a vial containing the growth solution. Subsequently, the vial was immersed in a water bath held at 90 ^{o}C for 30 minutes. The glass slide supported the template by leaning against the sidewall of the vial, resulting in no precipitation on the template. Then, the immersed template was removed from the growth solution, rinsed with DI water to get rid of any residual materials, and dried under ambient conditions. Fig. 1b (i, ii) shows scanning electron microscope (SEM) images of the aluminum template before and after the growth of ZnO nanostructures.

The growth of ZnO nanostructures in a substrate for a fixed precursor-base (zinc acetate-HMTA in this study) pair can be controlled by the surface roughness of template [61]. Therefore, we roughened aluminum templates by dipping those in 0.1M KOH solution for various times and grew the ZnO nanostructures. Etching created pits on aluminum; these pits restricted the free

movement of Zn atoms by trapping them, served as nucleation sites and promoted the growth of nanostructures [61].

One of the advantages of this method is that template can be reused by re-growing the

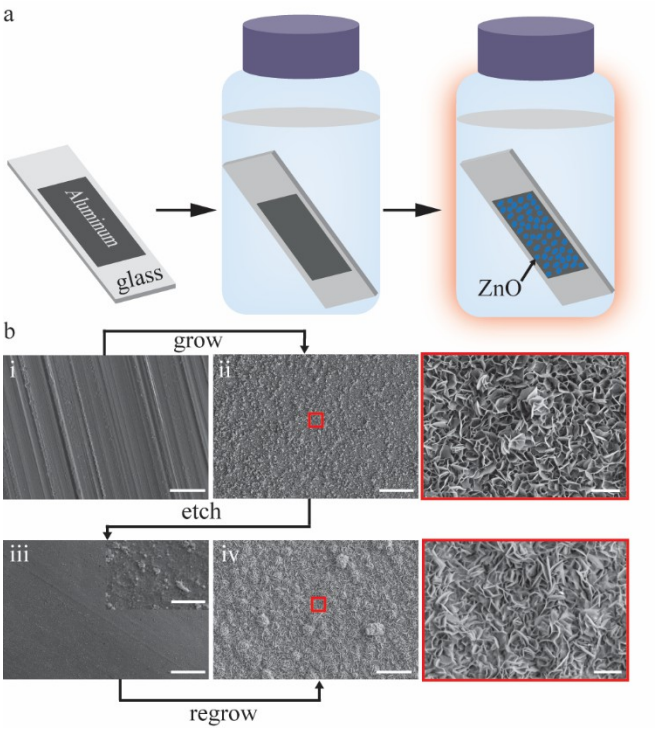

Fig. 1 Synthesis of ZnO nanostructures on aluminum template. (a) Schematic illustration of hydrothermal synthesis steps. The vial containing growth solution and aluminum template (attached with glass slide) was held at 90 °C. (b) SEM images of the aluminum template: (i) bare surface (scale bar 50 µm), (ii) after growing the ZnO nanostructures (scale bars 50 µm and 2 µm), (iii) after etching away the nanostructures (scale bar 100 µm, inset scale bar 5 µm), and (iv) after regrowing the ZnO nanostructures (scale bars 10 µm and 2 µm).

ZnO nanostructures. To do so, existing nanostructures were removed through chemical etching (0.1 M KOH solution) and the fresh ones were grown as discussed at the beginning of this section. Fig. 1b (iii, iv) shows the SEM images of aluminum surface after removing ZnO nanostructures and after growing the new ones.

2.2 Sacrificial Nanoimprint Lithography

For nanoimprinting TPE samples, we employed Kraton D1112, a styrene-butadiene-styrene triblock copolymer with 29.5 wt.% styrene content. Nanoimprinting has been widely used to

pattern MGs, and excellent reviews are available for further reading [62-64]. The sacrificial nanoimprinting process includes two steps: molding and demolding, as is shown in Fig. 2a. During molding, to compliant thermoplastic materials, they were heated above the glass transition temperature (T_g) embossed against the aluminum templates with ZnO nanostructures. The T_g of the styrenic glassy domains in the TPE is 110 ºC, and the molding was conducted at 120 ºC. Similarly, Pt-MG was molded 40 ºC above its T_g (220 ºC). Because of the softening nature of glasses above T_g, the ZnO nanostructures easily penetrated the surface, but broke and

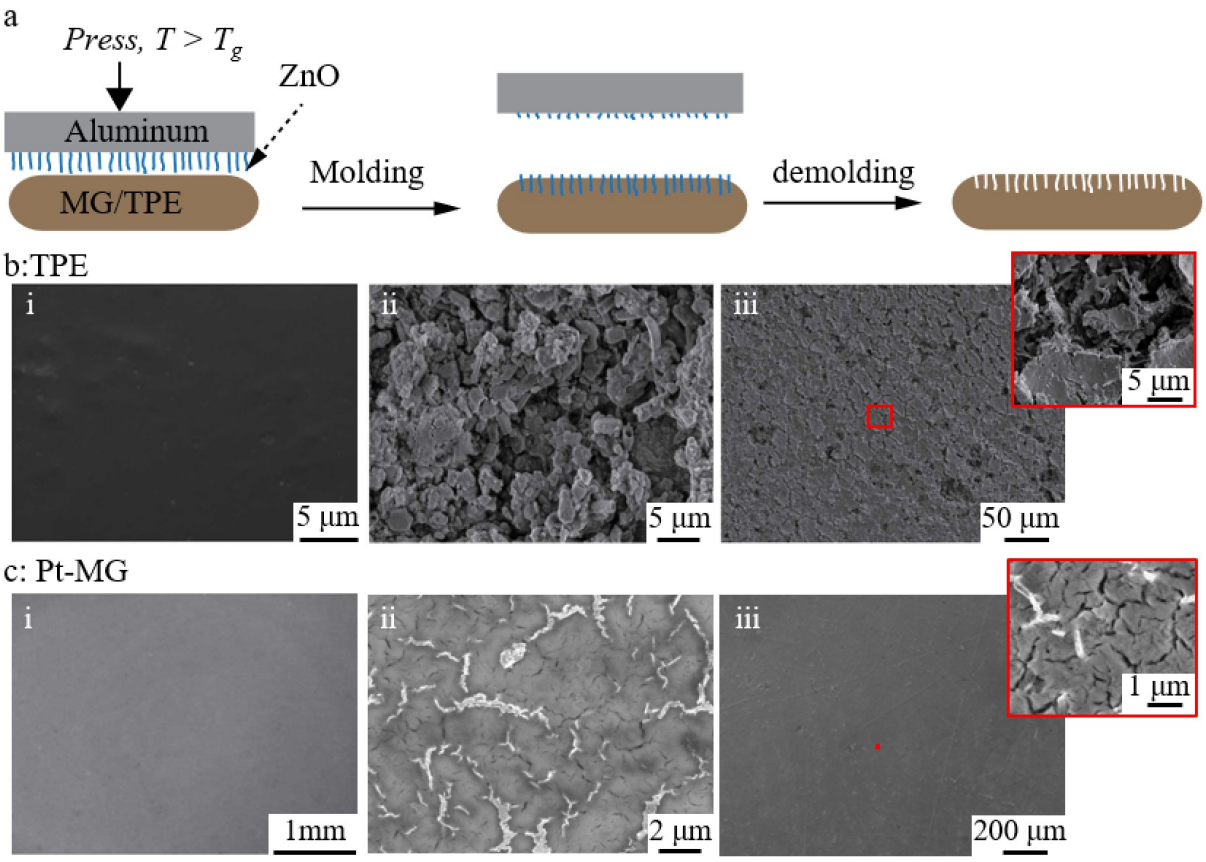

Fig. 2 Modifying the topography of TPE. (a) Schematic illustration of nanoimprinting. To imprint, both the template and the TPE were heated at 120 ºC (which is 10 ºC above the T_g of TPE) and pressed. ZnO nanostructures embedded in the TPE broke during demolding at room temperature. The broken nanostructures were removed through etching. (b) SEM images of TPE (Kraton) (i) of a bare surface, (ii) after embossing, and (ii) after etching. (c) SEM images of Pt-MG (i) of flat surface, (ii) after embossing, and (iii) after etching.

embedded in their surface during mechanical separation of the templates and the materials at room temperature. Therefore, demolding was carried out through dissolving the ZnO nanostructures in 0.5 M KOH solution, which left the desired surface porosity structures on the surface. Fig. 2b(iii) shows the multi-level porous structures after removing the ZnO nanostructures. The aluminum master template can be reused by dissolving the broken ZnO nanostructures in a mild base solution and growing the new ones as described in section 2.1.

2.3 Surface Characterization

The wettability of MG and TPE was measured using sessile drop method, in which 5 µl droplets of deionized water were dispensed onto the surfaces of MG and TPE using a micro-pipette and the static contact angle (CA) measurements were conducted using an optical tensiometer (OneAttension, Biolin scientific). The surface topography of MG and TPE were characterized using Zeiss Sigma FESEM scanning electron microscope (SEM).

3.0 Results and Discussion

To study the effect of roughness, Pt-MG was decorated with different topographies through SNIL. Table 1 lists the experimental parameters and resultant feature densities, with Fig. 3 displaying the results graphically. A non-textured Pt-MG surface is slightly hydrophilic (CA65°), similar to the value previously obtained for the same MG [65,66]. As compared to this initial state, the sacrificially templated structures show universally greater hydrophilicity, most likely arising from the hydrophilic enhancement of mesoscale roughness on hydrophilic surfaces [20,22] and oxidation as previously described [65,66]. A dominant characteristic size[1] was determined by Fourier analysis as the center of the transformed peak, with the CA trending strongly with this size. Another critical parameter was the classification of surfaces as "pore-like", with the MG presenting the continuous structure on the surface, or "pillar-like," with the

1 These are presented without vertical error bars for visualization, however, the range of apparent sizes for a majority of samples was equal to or greater than the average feature size.

void space presenting the continuous structure on the surface. Pillar-like structures exhibit lower CAs down to the super-hydrophilic regime, likely due to the increased ability for the pore-like structures to trap air. By utilizing the wide range of possible structures, tuning over the complete range of angles between the starting CA and fully wetting was demonstrated.

Table 1: MG Sample Preparation, CA, and Size for Pore (**Pillar**) Morphology

Preparation	CA (°)	Characteristic Size (μm)
Flat	64	0
260 Brass (low polish)	57	0.12
260 Brass (high polish)	**15**	**0.18**
353 Brass (low polish)	46	0.29
353 Brass (high polish)	64	0.21
Seeded Silicon	45	0.24
Silicon with 60 nm BCP	42	0.17
Silicon with 70 nm BCP	35	0.38
Silicon with 100 nm BCP	50	0.26
Silicon with 100 nm BCP Sparse	35	0.5
2024 Aluminum (high polish)	28	1.15
2024 Aluminum (high polish) with 100 nm BCP	**0**	**1.20**

We also pursued surface modification of TPEs for two reasons: (1) TPEs are ubiquitous forming materials in consumer goods, such as footwear and tires and (2) TPEs start from a hydrophobic surface and thus it was expected that they could be tuned to superhydrophobic. In pursuing TPE modification, we focused on Al-seeded growth modified by surface etching. The rational for this was four-fold: (1) aluminum molds showed the largest effects on CA in the MG results, (2) aluminum molds are readily fabricated, (3) etched surfaces are easier to produce than polished ones, and (4) repeatable Al-seeding from aluminum is more robust than Zn-seeding from brass. This last point may be understood due to the fact that cleaning and removal of the

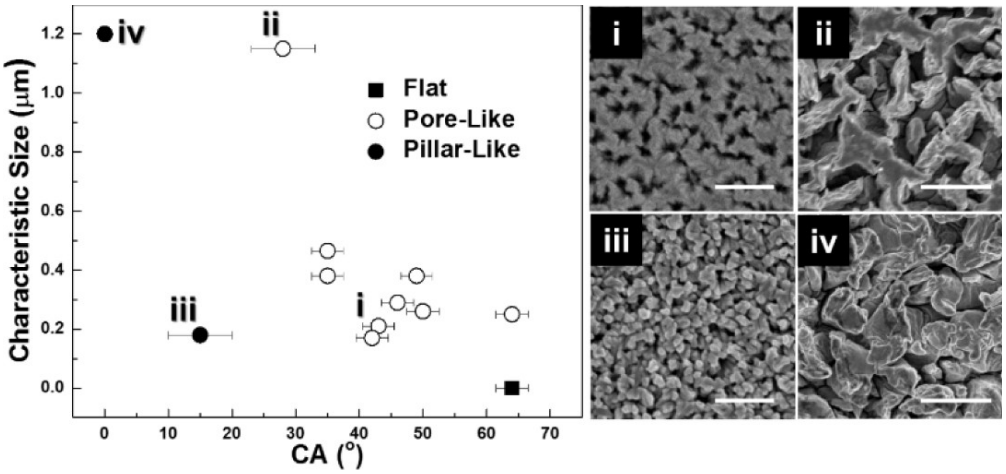

Fig. 3: Water CA alteration by sacrificial templating with different characteristic scales for both "pore-like" (i) and (ii) and "pillar-like" (iii) and (iv) geometries. Scale bars in (i) and (iii) are 500 nm and scale bars in (ii) and (iv) are 2 μm.

ZnO structures from a brass surface leaches the Zn from the brass surface, leaving copper and copper oxide, whereas an aluminum mold will always have excess Al for growth.

To control the wettability of the formed materials, we tuned their morphology through SNIL. Because this imprinting is template assisted, changing the density and the size of nanostructures on the template is an easy route to alter the topography of elastomer. Fig. 4a shows the effect of etching on the growth of ZnO nanostructures on aluminum templates with the three different base soaking times. Because of anisotropic growth along two planes: (0001) and (), nanoflake-like structures grew on the templates [67]. The density of the nanoflakes over the temples and their sizes, however, were different in these templates. Higher etching time allows to create more pits, resulting denser ZnO nanostructures during hydrothermal growth, but also overall sample roughness. Hence, the template exposed to KOH for 40 minutes had densest flake-like structures among the three templates, but also the roughest surface. To demonstrate the effect of ZnO nanostructures on the nanoimprinting of TPE and its consequence on wettability, we used templates with different immersion times (0-40 minutes) in KOH. Fig. 4b shows the SEM

images of flat and two nanoimprinted elastomers (TPE A and TPE B) and their corresponding photographs to measure water CAs. TPE A and TPE B were embossed with 20-minute etched and 40-minute etched templates,

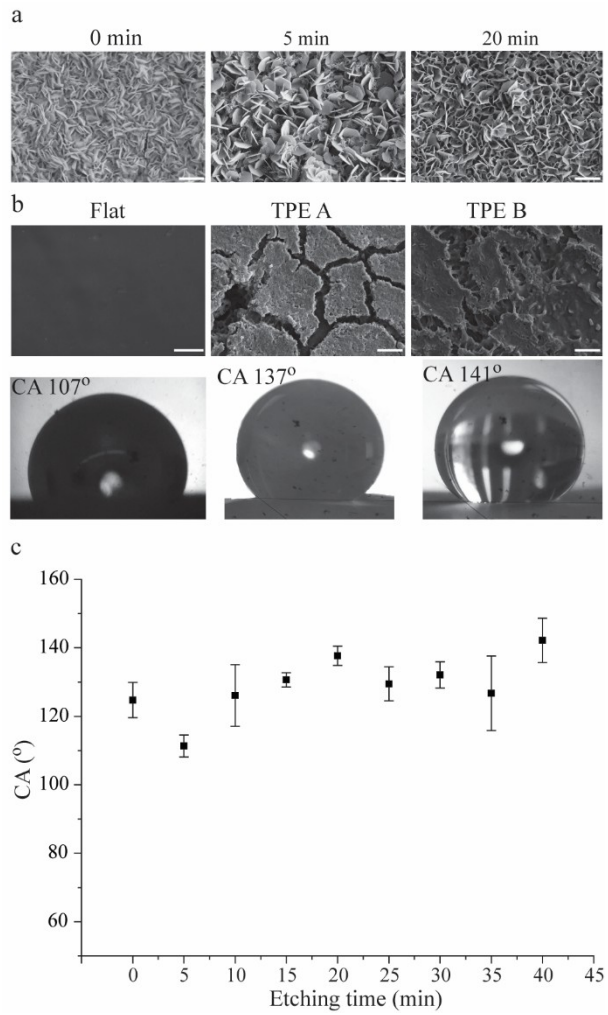

Fig. 4: Tuning the surface wettability of TPE. (a) SEM image of aluminum templates with ZnO nanostructures. The growth and density of the nanostructures are varied with the immersion time. (b) SEM images of flat and nanoimprinted TPEs and corresponding CA measurements. Scale bar is 2μm. (c) Effect of pretreatment of aluminum template on the wettability of TPE. The Cas measurement error is ±5°.

respectively. The plot in Fig. 4c quantifies the wettability of elastomer as a function of immersion time of the template in KOH solution. The flat elastomer is hydrophobic (CA > 90°) but surface patterning, after an initial decrease in the CA, increases CA up to 20 mins of etching

to a peak shown by TPE A (137^{o}). This increase may be understood by an increase in the characteristic size of the multiscale structuring as demonstrated in the MG results. Further etching results in a decrease of CA, as the overall roughness of the surface begins to affect the results. This then increases again up to the superhydrophobic CA shown by TPE B (141^{o} ± 5^{o}) at 40 min etching. Because TPE B was imprinted with the template which had both the densest nanostructures and multiscale roughness, the resulting surface with a high-level of pillar-like porosity.

The increase of CA (θ) can be explained by the Wenzel model, which is defined as follow [68]:

where r is surface roughness and θ_Y is the Young CA or intrinsic CA. Because θ_Y of the elastomer is greater than 90^{o}, increase in roughness (r) promotes the dewetting behavior of elastomer. Therefore, TPE samples prepared using the templates exposing to KOH for longer duration shows superhydrophobicity.

One of the advantages of SNIL is that it can be employed to make 3D superhydrophobic parts. To do so, we used an aluminum block with a rectangular cavity at the center (Fig. 5a) as a template. To grow ZnO nanostructures on the template and consequently, nanoimprint a 3D part, we followed the protocols described in section 2.1 and 2.2. The Fig. 5b shows the multiple water droplets rest on the different faces of the 3D part. All the faces except the bottom one show increased hydrophobicity (Fig. 5c-g); the bottom face was used to force the elastomer to fill the mold cavity during thermoplastic forming and did not come in contact with aluminum template. The left and right surfaces also show reduced CA as they were used to grip during removal from the mold and were damaged in the process. Although the droplets give higher CAs, they do not roll off of the

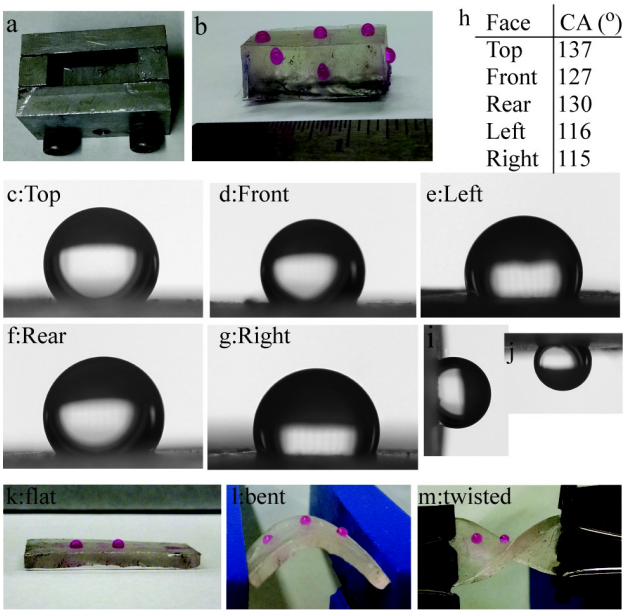

Face	CA (°)
Top	137
Front	127
Rear	130
Left	116
Right	115

Fig. 5: Superhydrophobic 3D TPE. (a) The aluminum mold for 3D imprinting. (b) Photographs of water droplets on the different faces of the superhydrophobic 3D part. (c-g) Water droplets on different faces of TPE. (h) Table of CAs of different faces. (i-j) water droplets rest on vertical and flipped TPE surfaces. (k-m) Optical images of water droplets on TPE substrate under flat, bending, and twisting. CA measurement error is ±5°.

vertical surfaces (Fig. 5i) and adhere to the surface even it is flipped (Fig. 5j) due to high adhesion. This phenomenon is known as petal effect [69].

The robustness of superhydrophobic materials depends on few factors, including the ability to withstand mechanical deformation. The nanostructures prerequisite for Cassie-Baxter wetting state and consequently high CA could collapse or enlarge when subject to strain due to bending, stretching, and twisting [70]. The distortion of nanostructures allows water to penetrate the surface to change wetting state form heterogenous to homogenous, increasing wettability. Because of higher elastic and plastic limits of TPE, the air-pockets formed by nanostructures do not rupture, and as a result, the hydrophobicity of TPE substrate remains unchanged when it undergoes deformations: bending and twisting (Fig. 5k-m). Such kind of flexible superhydrophobic materials has important applications in water-resistant flexible electronics [71], self-cleaning curved surfaces [72], and flexible microfluidics [73,74].

Conclusion

In summary, we demonstrated a practical fabrication method to control the wetting behavior of two different thermoplastic materials – TPE and Pt-MG – by modifying their topographies, with a larger characteristic size and multiscale roughness both enhancing the resulting surface property modification. The sacrificial nanoimprinting method demonstrated here combines the hydrothermal growth of ZnO nanostructures and thermoplastic embossing to create superhydrophilic and superhydrophobic materials. We showed that surface pretreatment of aluminum template dictated its topography and eventually, controlled the wettability of imprinted TPE. Uniform growth of ZnO nanostructures in a large area and the reusability of template make this method economical. Moreover, the method is compatible to tune the wettability of large and complex 3D parts. By changing the process parameters, sacrificial nanoimprinting may be extended to other inorganic and organic materials, which are thermoplastically moldable.

Acknowledgements

This work was supported by NSF MRSEC DMR-1119826, ONR YIP award N000141210657, and the Rutgers University School of Engineering. M. Hasan would like to acknowledge the Mistletoe Foundation through the Mistletoe Research Fellowship. The authors would also like to acknowledge support of the State of New Jersey through the New Jersey Governor's School for Engineering and Technology Program and Dean J. P. Antoine for coordination of this program.

References

[1] Kota, A. K., Kwon, G., Choi, W., Mabry, J. M., and Tuteja, A., 2012, "Hygro-Responsive Membranes for Effective Oil-Water Separation," Nat. Commun., **3**, p. 1025.

[2] Hermelin, E., Petitjean, J., Lacroix, J. C., Chane-Ching, K. I., Tanguy, J., and Lacaze, P. C., 2008, "Ultrafast Electrosynthesis of High Hydrophobic Polypyrrole Coatings on a Zinc Electrode: Applications to the Protection against Corrosion," Chem. Mater., **20**(13), pp. 4447-56.

[3] Tahk, D., Kim, T. I., Yoon, H., Choi, M., Shin, K., and Suh, K. Y., 2010, "Fabrication of Antireflection and Antifogging Polymer Sheet by Partial Photo Polymerization and Dry Etching," Langmuir, **26**(4), pp. 2240-43.

[4] Bhushan, B., and Jung, Y. C., 2011, "Natural and Biomimetic Artificial Surfaces for Superhydrophobicity, Self-Cleaning, Low Adhesion, and Drag Reduction," Prog. Mater. Sci., **56**(1), pp. 1-108.

[5] Drelich, J., Chibowski, E., Meng, D. D., and Terpilowski, K., 2011, "Hydrophilic and Superhydrophilic Surfaces and Materials," Soft Matter, **7**(21), pp. 9804-28.

[6] Zhang, X., Shi, F., Niu, J., Jiang, Y. G., and Wang, Z. Q., 2008, "Superhydrophobic Surfaces: From Structural Control to Functional Application," J. Mater. Chem., **18**(6), pp. 621-33.

[7] Roach, P., Shirtcliffe, N. J., and Newton, M. I., 2008, "Progess in Superhydrophobic Surface Development," Soft Matter, **4**(2), pp. 224-40.

[8] Chen, C. B., Li, R., Xu, L. M., and Yan, D. Y., 2014, "Three-Dimensional Superhydrophobic Porous Hybrid Monoliths for Effective Removal of Oil Droplets from the Surface of Water," RSC Adv., **4**(33), pp. 17393-400.

[9] Ruan, C. P., Shen, M. X., Ren, X. Y., Ai, K. L., and Lu, L. H., 2016, "A Versatile and Scalable Approach toward Robust Superhydrophobic Porous Materials with Excellent Absorbency and Flame Retardancy," Sci. Rep., **6**, 31233

[10] Bird, J. C., Dhiman, R., Kwon, H. M., and Varanasi, K. K., 2013, "Reducing the Contact Time of a Bouncing Drop," Nature, **503**(7476), pp. 385-88.

[11] Schutzius, T. M., Jung, S., Maitra, T., Graeber, G., Kohme, M., and Poulikakos, D., 2015, "Spontaneous Droplet Trampolining on Rigid Superhydrophobic Surfaces," Nature, **527**(7576), pp. 82-85.

[12] Boreyko, J. B., and Chen, C. H., 2009, "Self-Propelled Dropwise Condensate on Superhydrophobic Surfaces," Phy. Rev. Lett., **103**(18), p. 184501.

[13] Park, K. C., Kim, P., Grinthal, A., He, N., Fox, D., Weaver, J. C., and Aizenberg, J., 2016, "Condensation on Slippery Asymmetric Bumps," Nature, **531**(7592), pp. 78-82.

[14] Zhao, J., Zhang, X. B., Chen, N., and Pan, Q. M., 2012, "Why Superhydrophobicity Is Crucial for a Water-Jumping Microrobot? Experimental and Theoretical Investigations," ACS Appl. Mater. Interfaces, **4**(7), pp. 3706-11.

[15] Song, Y. S., and Sitti, M., 2007, "Surface-Tension-Driven Biologically Inspired Water Strider Robots: Theory and Experiments," IEE Trans. Robot., **23**(3), pp. 578-89.

[16] Zhu, X. T., Zhang, Z. Z., Ren, G. N., Yang, J., Wang, K., Xu, X. H., Men, X. H., and Zhou, X. Y., 2012, "A Novel Superhydrophobic Bulk Material," J. Mater. Chem., **22**(38), pp. 20146-48.

[17] Ji, K. J., Liu, J., Zhang, J., Chen, J., and Dai, Z. D., 2014, "Super-Floatable Multidimensional Porous Metal Foam Integrated with a Bionic Superhydrophobic Surface," J. Mater. Chem. A, **2**(39), pp. 16589-93.

[18] Bhushan, B., Jung, Y. C., and Koch, K., 2009, "Micro-, Nano- and Hierarchical Structures for Superhydrophobicity, Self-Cleaning and Low Adhesion," Phil. Trans. R. Soc. A, **367**(1894), pp. 1631-72.

[19] Fan, J. G., Tang, X. J., and Zhao, Y. P., 2004, "Water Contact Angles of Vertically Aligned Si Nanorod Arrays," Nanotechnology, **15**(5), pp. 501-04.

[20] Bhushan, B., Jung, Y. C., and Koch, K., 2009, "Self-Cleaning Efficiency of Artificial Superhydrophobic Surfaces," Langmuir, **25**(5), pp. 3240-48.

[21] Rupp, F., Scheideler, L., Rehbein, D., Axmann, D., and Geis-Gerstorfer, J., 2004, "Roughness Induced Dynamic Changes of Wettability of Acid Etched Titanium Implant Modifications," Biomaterials, **25**(7-8), pp. 1429-38.

[22] Bico, J., Tordeux, C., and Quere, D., 2001, "Rough Wetting," Europhys. Lett., **55**(2), pp. 214-20.

[23] Sabbah, A., Youssef, A., and Damman, P., 2016, "Superhydrophobic Surfaces Created by Elastic Instability of Pdms," Appl. Sci., **6**(5), pp. 152.

[24] Kawai, A., and Nagata, H., 1994, "Wetting Behavior of Liquid on Geometrical Rough-Surface Formed by Photolithography," Jpn. J. Appl. Phys. Part 2, **33**(9A), pp. L1283-L85.

[25] Shirtcliffe, N. J., Aqil, S., Evans, C., McHale, G., Newton, M. I., Perry, C. C., and Roach, P., 2004, "The Use of High Aspect Ratio Photoresist (Su-8) for Super-Hydrophobic Pattern Prototyping," J. Micromech. Microeng., **14**(10), pp. 1384-89.

[26] Xia, Y., Kim, E., Zhao, X.-M., Rogers, J. A., Prentiss, M., and Whitesides, G. M., 1996, "Complex Optical Surfaces Formed by Replica Molding against Elastomeric Masters," Science, **273**(5273), pp. 347-49.

[27] Xu, B., Arias, F., Brittain, S. T., Zhao, X. M., Grzybowski, B., Torquato, S., and Whitesides, G. M., 1999, "Making Negative Poisson's Ratio Microstructures by Soft Lithography," Adv. Mater., **11**(14), pp. 1186-89.

[28] Singer, J. P., Pelligra, C. I., Kornblum, N., Choo, Y., Gopinadhan, M., Bordeenithikasem, P., Ketkaew, J.*, et al.*, 2015, "Multiscale Patterning of a Metallic Glass Using Sacrificial Imprint Lithography," Microsyst. Nanoeng., **1**, 15040.

[29] Singer, J. P., Gopinadhan, M., Shao, Z., Taylor, A. D., Schroers, J., and Osuji, C. O., 2015, "Nanoimprinting Sub-100 Nnn Features in a Photovoltaic Nanocomposite Using Durable Bulk Metallic Glass Molds," ACS Appl. Mater. Interfaces, **7**(6), pp. 3456-61.

[30] Busscher, H. J., Stokroos, I., Vandermei, H. C., Rouxhet, P. G., and Schakenraad, J. M., 1992, "Preparation and Characterization of Superhydrophobic Fep-Teflon Surfaces," J. Adhes. Sci. Technol., **6**(3), pp. 347-56.

[31] Zhang, X., Jin, M., Liu, Z., Nishimoto, S., Saito, H., Murakami, T., and Fujishima, A., 2006, "Preparation and Photocatalytic Wettability Conversion of Tio2-Based Superhydrophobic Surfaces," Langmuir, **22**(23), pp. 9477-79.

[32] Li, X. H., Chen, G. M., Ma, Y. M., Feng, L., Zhao, H. Z., Jiang, L., and Wang, F. S., 2006, "Preparation of a Super-Hydrophobic Poly(Vinyl Chloride) Surface Via Solvent-Nonsolvent Coating," Polymer, **47**(2), pp. 506-09.

[33] Han, J. T., Xu, X. R., and Cho, K. W., 2005, "Diverse Access to Artificial Superhydrophobic Surfaces Using Block Copolymers," Langmuir, **21**(15), pp. 6662-65.

[34] Karuppuchamy, S., and Jeong, J. M., 2005, "Super-Hydrophilic Amorphous Titanium Dioxide Thin Film Deposited by Cathodic Electrodeposition," Mater. Chem. Phys., **93**(2-3), pp. 251-54.

[35] Satyaprasad, A., Jain, V., and Nema, S. K., 2007, "Deposition of Superhydrophobic Nanostructured Teflon-Like Coating Using Expanding Plasma Arc," Appl. Surf. Sci., **253**(12), pp. 5462-66.

[36] Genzer, J., and Efimenko, K., 2000, "Creating Long-Lived Superhydrophobic Polymer Surfaces through Mechanically Assembled Monolayers," Science, **290**(5499), pp. 2130-33.

[37] Song, X. Y., Zhai, J., Wang, Y. L., and Jiang, L., 2005, "Fabrication of Superhydrophobic Surfaces by Self-Assembly and Their Water-Adhesion Properties," J. Phy. Chem. B, **109**(9), pp. 4048-52.

[38] Pozzato, A., Dal Zilio, S., Fois, G., Vendramin, D., Mistura, G., Belotti, M., Chen, Y., and Natali, M., 2006, "Superhydrophobic Surfaces Fabricated by Nanoimprint Lithography," Microelectron. Eng., **83**(4-9), pp. 884-88.

[39] Lee, S. M., and Kwon, T. H., 2006, "Mass-Producible Replication of Highly Hydrophobic Surfaces from Plant Leaves," Nanotechnology, **17**(13), pp. 3189-96.

[40] Radha, B., Lim, S. H., Saifullah, M. S. M., and Kulkarni, G. U., 2013, "Metal Hierarchical Patterning by Direct Nanoimprint Lithography," Sci. Rep., **3**, 1078.

[41] Boinovich, L., Emelyanenko, A. M., and Pashinin, A. S., 2010, "Analysis of Long-Term Durability of Superhydrophobic Properties under Continuous Contact with Water," ACS Appl. Mater. & Interfaces, **2**(6), pp. 1754-58.

[42] Ellis, D. A., Mabury, S. A., Martin, J. W., and Muir, D. C. G., 2001, "Thermolysis of Fluoropolymers as a Potential Source of Halogenated Organic Acids in the Environment," Nature, **412**(6844), pp. 321-24.

[43] Johansson, N., Fredriksson, A., and Eriksson, P., 2008, "Neonatal Exposure to Perfluorooctane Sulfonate (Pfos) and Perfluorooctanoic Acid (Pfoa) Causes Neurobehavioural Defects in Adult Mice," Neurotoxicology, **29**(1), pp. 160-69.

[44] Suja, F., Pramanik, B. K., and Zain, S. M., 2009, "Contamination, Bioaccumulation and Toxic Effects of Perfluorinated Chemicals (Pfcs) in the Water Environment: A Review Paper," Water Sci. Technol., **60**(6), pp. 1533-44.

[45] Song, W., Zhang, J., Xie, Y., Cong, Q., and Zhao, B., 2009, "Large-Area Unmodified Superhydrophobic Copper Substrate Can Be Prepared by an Electroless Replacement Deposition," J. Colloid Interf. Sci., **329**(1), pp. 208-11.

[46] Shirtcliffe, N. J., McHale, G., Newton, M. I., Chabrol, G., and Perry, C. C., 2004, "Dual-Scale Roughness Produces Unusually Water-Repellent Surfaces," Adv. Mater., **16**(21), pp. 1929-32.

[47] Baruah, S., and Dutta, J., 2009, "Hydrothermal Growth of Zno Nanostructures," Sci. Technol. Adv. Mat., **10**(1), pp. 013001.

[48] Vayssieres, L., Keis, K., Lindquist, S. E., and Hagfeldt, A., 2001, "Purpose-Built Anisotropic Metal Oxide Material: 3d Highly Oriented Microrod Array of Zno," J. Phys. Chem. B, **105**(17), pp. 3350-52.

[49] Verges, M. A., Mifsud, A., and Serna, C. J., 1990, "Formation of Rod-Like Zinc-Oxide Microcrystals in Homogeneous Solutions," J. Chem. Soc. Faraday Trans., **86**(6), pp. 959-63.

[50] Abdelfatah, M., and El-Shaer, A., 2018, "One Step to Fabricate Vertical Submicron Zno Rod Arrays by Hydrothermal Method without Seed Layer for Optoelectronic Devices," Mater. Lett., **210**), pp. 366-69.

[51] Kim, S., Kim, M. S., Park, H., Nam, G., Yoon, H., and Leem, J. Y., 2014, "Seed-Layer-Free Hydrothermal Growth of Zinc Oxide Nanorods on Porous Silicon," Electron. Mater. Lett., **10**(3), pp. 565-71.

[52] Fan, X., Fang, G. J., Guo, S. S., Liu, N. S., Gao, H. M., Qin, P. L., Li, S. Z.*, et al.*, 2011, "Controllable Synthesis of Flake-Like Al-Doped Zno Nanostructures and Its Application in Inverted Organic Solar Cells," Nanoscale Res. Lett., **6**), pp. 546.

[53] Xia, T., Li, N., Wu, Y., and Liu, L., 2012, "Patterned Superhydrophobic Surface Based on Pd-Based Metallic Glass," Appl. Phys. Lett., **101**(8), pp. 081601.

[54] Li, N., Xia, T., Heng, L., and Liu, L., 2013, "Superhydrophobic Zr-Based Metallic Glass Surface with High Adhesive Force," Appl. Phys. Lett., **102**(25), pp. 251603.

[55] Arora, H. S., Xu, Q., Xia, Z., Ho, Y. H., Dahotre, N. B., Schroers, J., and Mukherjee, S., 2013, "Wettability of Nanotextured Metallic Glass Surfaces," Scripta Mater., **69**(10), pp. 732-35.

[56] Zhao, K., Liu, K. S., Li, J. F., Wang, W. H., and Jiang, L., 2009, "Superamphiphobic Cali-Based Bulk Metallic Glasses," Scripta Mater., **60**(4), pp. 225-27.

[57] Liu, K., Li, Z., Wang, W., and Jiang, L., 2011, "Facile Creation of Bio-Inspired Superhydrophobic Ce-Based Metallic Glass Surfaces," Appl. Phys. Lett., **99**(26), pp. 261905.

[58] Gao, M., Wang, D. P., Huang, Y. F., Meng, S., and Wang, W. H., 2016, "Tunable Hydrophobicity on Fractal and Micro-Nanoscale Hierarchical Fracture Surface of Metallic Glasses," Mater. Des., **95**), pp. 612-17.

[59] Huang, L., Pu, C., Fisher, R. K., Mountain, D. J. H., Gao, Y. F., Liaw, P. K., Zhang, W., and He, W., 2015, "A Zr-Based Bulk Metallic Glass for Future Stent Applications: Materials Properties, Finite Element Modeling, and in Vitro Human Vascular Cell Response," Acta Biomaterialia, **25**), pp. 356-68.

[60] Schroers, J., and Johnson, W. L., 2004, "Ductile Bulk Metallic Glass," Phys. Rev. Lett., **93**(25), p. 255506.

[61] Roozbehi, M., Sangpour, P., Khademi, A., and Moshfegh, A. Z., 2011, "The Effect of Substrate Surface Roughness on Zno Nanostructures Growth," Appl. Surf. Sci., **257**(8), pp. 3291-97.

[62] Schroers, J., 2005, "The Superplastic Forming of Bulk Metallic Glasses," JOM, **57**(5), pp. 35-39.

[63] Li, N., Chen, W., and Liu, L., 2016, "Thermoplastic Micro-Forming of Bulk Metallic Glasses: A Review," JOM, **68**(4), pp. 1246-61.

[64] Schroers, J., 2010, "Processing of Bulk Metallic Glass," Adv. Mater., **22**(14), pp. 1566-97.

[65] Hasan, M., Warzywoda, J., and Kumar, G., 2018, "Decoupling the Effects of Surface Texture and Chemistry on the Wetting of Metallic Glasses," Appl. Surf. Sci., **447**), pp. 355-62.

[66] Hasan, M., "Decoupling the Effects of Surface Roughness and Chemistry on the Wetting of Metallic Glasses." Texas Tech University, 2017.

[67] Pawar, R. C., Kim, H., and Lee, C. S., 2014, "Defect-Controlled Growth of Zno Nanostructures Using Its Different Zinc Precursors and Their Application for Effective Photodegradation," Curr. Appl. Phys., **14**(4), pp. 621-29.

[68] Wenzel, R. N., 1949, "Surface Roughness and Contact Angle," J. Phys. Chem., **53**(9), pp. 1466-67.

[69] Bhushan, B., and Nosonovsky, M., 2010, "The Rose Petal Effect and the Modes of Superhydrophobicity," Philosophical Transactions of the Royal Society a-Mathematical Physical and Engineering Sciences, **368**(1929), pp. 4713-28.

[70] Wang, Y. Q., Shi, Y., Pan, L. J., Yang, M., Peng, L. L., Zong, S., Shi, Y., and Yu, G. H., 2014, "Multifunctional Superhydrophobic Surfaces Templated from Innately Microstructured Hydrogel Matrix," Nano Lett., **14**(8), pp. 4803-09.

[71] Lee, S., Kim, W., and Yong, K., 2011, "Overcoming the Water Vulnerability of Electronic Devices: A Highly Water-Resistant Zno Nanodevice with Multifunctionality," Adv. Mater., **23**(38), pp. 4398-402.

[72] Hao, X. Q., Wang, L., Lv, D. H., Wang, Q. D., Li, L., He, N., and Lu, B. H., 2015, "Fabrication of Hierarchical Structures for Stable Superhydrophobicity on Metallic Planar and Cylindrical Inner Surfaces," Appl. Surf. Sci., **325**), pp. 151-59.

[73] Yuen, P. K., and DeRosa, M. E., 2011, "Flexible Microfluidic Devices with Three-Dimensional Interconnected Microporous Walls for Gas and Liquid Applications," Lab Chip, **11**(19), pp. 3249-55.

[74] Seo, J., Lee, S. K., Lee, J., Lee, J. S., Kwon, H., Cho, S. W., Ahn, J. H., and Lee, T., 2015, "Path-Programmable Water Droplet Manipulations on an Adhesion Controlled Superhydrophobic Surface," Sci. Rep., **5**, 12326

List of Figure Caption:

Fig. 1 Synthesis of ZnO nanostructures on aluminum template. (a) Schematic illustration of hydrothermal synthesis steps. The vial containing growth solution and aluminum template (attached with glass slide) was held at 90 oC. (b) SEM images of the aluminum template: (i) bare surface (scale bar 50 μm), (ii) after growing the ZnO nanostructures (scale bars 50 μm and 2 μm), (iii) after etching away the nanostructures (scale bar 100 μm, inset scale bar 5 μm), and (iv) after regrowing the ZnO nanostructures (scale bars 10 μm and 2 μm).

Fig. 2 Modifying the topography of TPE. (a) Schematic illustration of nanoimprinting. To imprint, both the template and the TPE were heated at 120 oC (which is 10 oC above the Tg of TPE) and pressed. ZnO nanostructures embedded in the TPE broke during demolding at room temperature. The broken nanostructures were removed through etching. (b) SEM images of TPE (Kraton) (i) of a bare surface, (ii) after embossing, and (ii) after etching. (c) SEM images of Pt-MG (i) of flat surface, (ii) after embossing, and (iii) after etching.

Fig. 3: Water CA alteration by sacrificial templating with different characteristic scales for both "pore-like" (i) and (ii) and "pillar-like" (iii) and (iv) geometries. Scale bars in (i) and (iii) are 500 nm and scale bars in (ii) and (iv) are 2 μm.

Fig. 4: Tuning the surface wettability of TPE. (a) SEM image of aluminum templates with ZnO nanostructures. The growth and density of the nanostructures are varied with the immersion time. (b) SEM images of flat and nanoimprinted TPEs and corresponding CA measurements. Scale bar is 2μm. (c) Effect of pretreatment of aluminum template on the wettability of TPE. The Cas measurement error is ±5o.

Fig. 5: Superhydrophobic 3D TPE. (a) The aluminum mold for 3D imprinting. (b) Photographs of water droplets on the different faces of the superhydrophobic 3D part. (c-g) Water droplets on different faces of TPE. (h) Table of CAs of different faces. (i-j) water droplets rest on vertical and flipped TPE surfaces. (k-m) Optical images of water droplets on TPE substrate under flat, bending, and twisting. CA measurement error is ±5⌗.

List of Table Caption:

Table 1: MG Sample Preparation, CA, and Size for Pore (**Pillar**) Morphology